New Journal of Physics
The open access journal at the forefront of physics

Deutsche Physikalische Gesellschaft DPG IOP Institute of Physics

PAPER • OPEN ACCESS

Coherent charge and spin density waves in underdoped $HgBa_2CuO_{4+\delta}$

To cite this article: Jeongseop A Lee *et al* 2017 *New J. Phys.* **19** 033024

New Journal of Physics
The open access journal at the forefront of physics

Deutsche Physikalische Gesellschaft DPG
IOP Institute of Physics

Published in partnership with: Deutsche Physikalische Gesellschaft and the Institute of Physics

OPEN ACCESS

RECEIVED
17 November 2016

REVISED
9 February 2017

ACCEPTED FOR PUBLICATION
23 February 2017

PUBLISHED
16 March 2017

PAPER

Coherent charge and spin density waves in underdoped $HgBa_2CuO_{4+\delta}$

Jeongseop A Lee[1,4], Yizhou Xin[1], W P Halperin[1], A P Reyes[2], P L Kuhns[2] and M K Chan[3]

[1] Department of Physics and Astronomy Northwestern University, Evanston, IL 60208, United States of America
[2] National High Magnetic Field Laboratory, Tallahassee, FL 32310, United States of America
[3] Pulsed Field Facility, National High Magnetic Field Laboratory, Los Alamos National Laboratory, Los Alamos, NM 87545, United States of America
[4] Author to whom any correspondence should be addressed.

E-mail: jalee@u.northwestern.edu

Keywords: nuclear magnetic resonance, cuprates, charge density waves, spin density waves, pseudogap, superconductivity, Hg1201

Abstract

Charge order in cuprate superconductors appears to be a universal characteristic, often associated with pseudogap behavior in the normal state. The central question is whether such charge ordering or the pseudogap are required for the existence of high temperature superconductivity and embody its mechanism. An important but phenomenological approach to this question is to examine whether these phenomena extend over various members of the cuprate family. Recent nuclear magnetic resonance (NMR) measurements on oxygen chain-ordered single crystals of $YBa_2Cu_3O_{6+y}$ (Y123) have demonstrated temperature and magnetic field induced charge ordering that was confirmed in x-ray experiments. In the present work on high-quality single crystals of the tetragonal compound, $HgBa_2CuO_{4+\delta}$, we use ^{17}O NMR to investigate the interplay between charge and spin order deduced from the full quadrupolar-split NMR spectrum over a wide range of temperature and magnetic field. We have found evidence for a coherent modulation of charge and spin order in this compound. However, neither temperature nor magnetic field induced ordering was observed and we infer that this aspect of high temperature superconductivity is not universal.

1. Introduction

Various forms of spin and charge ordering have been identified in a wide range of cuprate superconducting materials, but whether these behaviors are ubiquitous phenomena is not established. In this work we focus on one of the simplest compounds, $HgBa_2CuO_{4+\delta}$ (Hg1201), a superconductor with a high transition temperature, 97 K, having only a single layer and tetragonal structure, in contrast to one of the most extensively studied materials, $YBa_2Cu_3O_{6+y}$ (Y123) [1–5]. Using nuclear magnetic resonance (NMR) we have discovered a coherent spatial modulation of both spin and charge that is temperature and magnetic field independent. However, there is no evidence for the magnetic field and temperature induced charge order observed in Y123 [1, 5]. Electronic instabilities are a common feature of cuprates [6] as in the present work on Hg1201, but their manifestations are not universal.

Efforts to better understand cuprate superconductors have focused on the nature of the pseudogap at temperatures above the superconducting transition and the role of spatial modulations of charge or spin [1–8]. A notable example is high-quality, underdoped crystals of Y123 [9]. Magnetic field and temperature induced charge order has been reported from NMR measurements [1, 4], recently confirmed as incommensurate by x-ray diffraction [5] in Y123 near hole-doping $p = 0.125$. This behavior can be correlated with change in sign of the temperature dependence in the Hall coefficient [10, 11], shown in the phase diagram figure 1, that has been associated with reconstruction of the Fermi surface with electron pockets identified from quantum oscillations [12, 13].

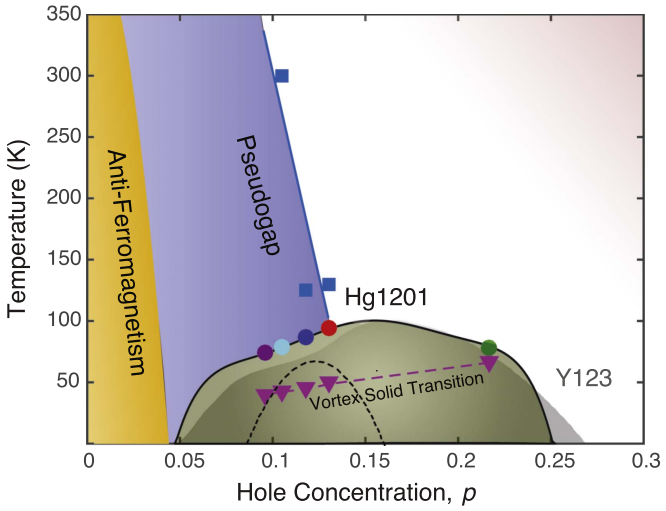

Figure 1. Phase diagram for Hg1201 taken in part from Yamamoto, *et al* [15, 19]. Vortex melting and pseudogap temperatures were determined from ^{63}Cu and ^{17}O NMR [20]. NMR results discussed in this report are for crystals (from left to right) UD74, UD79, and UD87 indicated by solid circles, together with two additional samples UD94 and OD89. The shaded dome in the background is for Y123 juxtaposed with a dashed parabolic curve indicating change in temperature dependence of the Hall coefficient [10, 11].

2. Experiment

We use ^{17}O NMR to investigate the underdoped high temperature cuprate Hg1201; a tetragonal, single layer compound with optimal superconducting transition of 97 K, arguably the simplest known high temperature superconductor. Similar to earlier NMR results on underdoped Y123 [1, 4], we have found charge and spin density wave order in Hg1201. However, distinct from the work in Y123 this order has a rather different character. It is temperature and magnetic field independent and it is not induced by either. This wide range of behaviors suggests that electronic ordering and superconductivity may not be intimately connected.

Crystals of near optimally doped Hg1201 were grown at the University of Minnesota. Isotope exchange for ^{17}O NMR was performed at Northwestern University followed by annealing for typically one week to establish doping and homogeneity. This report is mainly concerned with two underdoped single crystals of Hg1201 with $T_c = 87$ K (UD87) and 79 K (UD79) with the transition widths, $\Delta T_c = 5$ K and 1.5 K, respectively, measured by a low field superconducting quantum interference device, but with some work on the sample 74 K (UD74) with $\Delta T_c = 5$ K which we had reported upon previously [14]. Their oxygen concentrations correspond to hole doping of $p = 0.118, 0.105$, and 0.095 respectively, obtained by comparing the measured T_c with the phase diagram, figure 1 [15]. Additional characterization on these samples was performed by ^{199}Hg NMR which has revealed that in Hg1201 the interstitial dopant oxygens are randomly distributed in the Hg plane [16–18]. With perfect alignment of the crystal *c*-axis to the external field, there exists two sets of five ^{17}O NMR spectral peaks: one set for oxygen in the CuO_2 plane O(1), and the other for the apical oxygen O(2). Since the nuclear spin is $I = 5/2$, these are associated with the central transition, $\left(\frac{1}{2}, -\frac{1}{2}\right)$, and four quadrupolar satellites corresponding to the transitions, $\left(\frac{5}{2}, \frac{3}{2}\right)$, $\left(\frac{3}{2}, \frac{1}{2}\right)$, $\left(-\frac{1}{2}, -\frac{3}{2}\right)$, and $\left(-\frac{3}{2}, -\frac{5}{2}\right)$. In general the transition frequencies are labeled by indices $(m, m-1)$. For this investigation we have varied the magnetic field from $H_0 = 6$ to 30 T over a range of temperature, from ~4 to 400 K.

The situation where the magnetic field is not aligned with the *c*-axis is not D4 symmetric for O(1), resulting in anisotropic broadening or splitting of each of the peaks of the NMR spectrum since the two planar oxygens have orthogonal Cu-O bonding directions and are no longer degenerate. Therefore the O(1) rotation pattern consists of two sets of five peaks, one each for O(1a) and O(1b) where a and b denote one of two inequivalent oxygen sites in the cuprate plaquette identified by their differing projections of the magnetic field along the Cu–O bond. In contrast all apical sites O(2) are equivalent and their spectra always have exactly five peaks. This situation is very different from oxygen chain-ordered Y123 [1].

Additionally, the quadrupolar NMR spectra in a magnetic field will be modified in the presence of electronic charge or spin order. In the case of a change in the electronic spin susceptibility, all five spectral peaks of a given nucleus are affected identically and have the same shift in frequency. In contrast, charge order produces a modulation of the local electric field gradient (EFG) which changes the quadrupolar satellite frequencies shifting

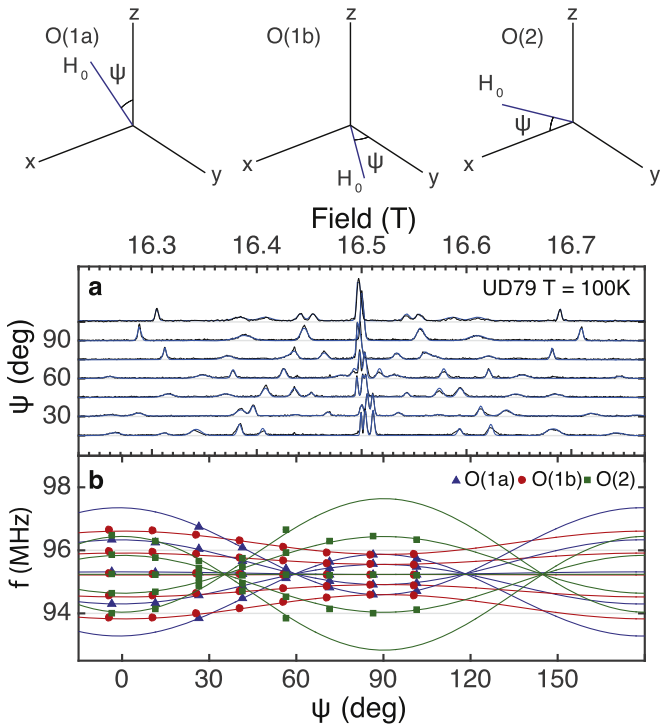

Figure 2. (a) NMR field swept spectra of UD79 at multiple orientations at $f = 95.39$ MHz, $H_0 = 16.5$ T, and $T = 80$ K with gaussian fits over each peak in blue lines with rotation about the b-axis. (b) Peak frequency positions of spectra for O(1a), O(1b), and O(2) as a function of ψ. Solid curves are fits described in the text.

them mirror-like with respect to the central peak. In short, spin or charge order can be independently identified from their distinct signatures in the NMR spectrum.

Given the various possible contributions to frequency shifts it is clear that to perform an NMR investigation of charge or spin ordering one must begin with a full determination of the rotation pattern as shown in figure 2 such that the crystal orientation can be completely understood prior to the measurement. Since the effects of charge order or spin order are at most relatively small compared to those associated with intrinsic anisotropy of the material, the absolute orientation of the crystals can be determined from the measured rotation pattern of the full quadrupolar spectrum, obtained using a single-axis goniometer, interpreted through fitting to the exact diagonalization of the nuclear spin Hamiltonian [21]. In this way we were able to align the c-axis close to the external field, H_0, with accuracy $(\delta\theta, \delta\phi) = (\pm 1^\circ, \pm 2^\circ)$. In this range, the expected upper bound for splitting of O(1) into O(1a) and O(1b) is ~2 kHz and less than the typical resolution of the NMR experiment, precluding crystal misalignment as the source for any observed frequency shifts.

The frequencies of satellites for less than axial symmetry as for O(1) are given explicitly by a summation of magnetic and quadrupolar contributions in the high magnetic field limit [21],

$$f(\theta, \phi, m) = f_{\text{mag}} + f^{(1)}_{\text{quad}} + f^{(2)}_{\text{quad}}, \tag{1}$$

$$f_{\text{mag}} = \gamma H_0 \left(1 + K_0 + K_1 \frac{(3\cos^2\theta - 1)}{2} - K_2 \frac{\sin^2\theta \cos 2\phi}{2}\right), \tag{2}$$

$$f^{(1)}_{\text{quad}} = \nu_Q \left(m - \frac{1}{2}\right)\left[\frac{(3\cos^2\theta - 1)}{2} - \eta \frac{\sin^2\theta \cos 2\phi}{2}\right]. \tag{3}$$

The magnetic and the first order quadrupolar contributions are given by equations (2) and (3), respectively. The second order quadrupolar contribution is given separately in appendix A. The gyromagnetic ratio for ^{17}O is $\gamma = 5.7719$ MHz/T, which we take as the zero reference for the Knight shift, K_0. The quadrupolar frequency ν_Q is proportional to the principal component of the EFG,

$$\frac{\partial^2 V}{\partial z^2} = \frac{\nu_Q 2I(2I-1)h}{3eQ} \geqslant \frac{\partial^2 V}{\partial y^2} \geqslant \frac{\partial^2 V}{\partial x^2}, \tag{4}$$

where V is the electrostatic potential, Q the quadrupole moment of the nucleus, and the principal axes, x, y, and z, for the EFG are chosen to satisfy these inequalities. The three eigenvalues of the EFG tensor are proportional to

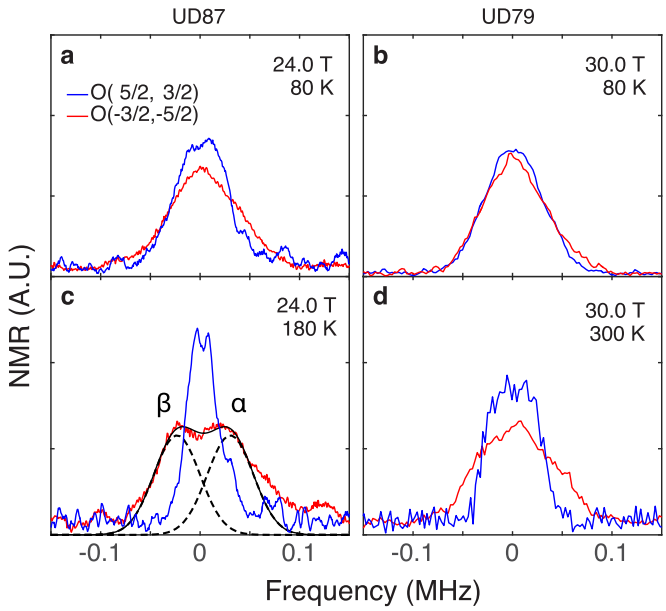

Figure 3. (a), (b) Examples of NMR spectra from the highest (red) and the lowest (blue) frequency satellites of the planar oxygen at two temperatures and fields parallel to the *c*-axis. Linewidth asymmetry between upper and lower frequency satellites for O(1), most significant at high temperatures, requires coexistence of spatially resolved spin and charge order. The α peak is defined as the higher frequency component and the β peak as the lower one of the doublet, remaining so at all fields and temperatures for all upper satellites. The same is not true for the lower satellites and the two peaks can merge forming substantially narrower compound spectra, as shown in c). The linewidth asymmetry is also directly reflected in peak intensity asymmetry, and can be seen clearly in the full spectrum of UD74 shown in figure 5. Similar asymmetry was reported by Kambe *et al* [23] for NMR spectra on grain aligned powder samples of $Tl_2Ba_2CuO_y$ and by Haase *et al* [24] for similar type samples of $La_{1.85}Sr_{0.15}CuO_4$ (LSCO). The latter group interpreted their results as possible evidence for charge and spin order.

the quadrupole frequency ν_Q with the *z*-axis along the Cu-O bond direction. The $2I + 1$ quadrupolar perturbed Zeeman substates are indexed by *m*. The superscript in the quadrupolar frequency distinguishes between 1st and 2nd order terms from perturbation theory in the high field limit. The form of the second order correction (appendix A) was included in our full analysis of the spectrum but has a negligible contribution to the frequency shifts, $\lesssim$1 kHz. The EFG anisotropy parameter is $\eta \equiv (\partial^2 V/\partial x^2 - \partial^2 V/\partial y^2)/(\partial^2 V/\partial z^2)$. Lastly, the polar and azimuthal angles, θ and ϕ, denote the orientation of H_0 with respect to *x*-, *y*-, *z*-axes.

For less than axial symmetry, as for O(1), the components of the Knight shift are measured with magnetic field along crystal axes, K_a, K_b, and K_c and can be expressed as isotropic, K_0, and axial shifts, K_1 and K_2. For O(1), $K_0 = (K_a + K_b + K_c)/3$; $K_1 = (2K_a - K_b - K_c)/3$; $K_2 = K_b - K_c \equiv \epsilon K_1$. In contrast O(2), the apical oxygen site well-removed from the copper-oxygen plane, has axial symmetry along the *c*-axis and the anisotropy ratio, ϵ, is zero. Using ^{17}O NMR at the apical site of UD74 we reported previously there was no evidence for static loop currents or for charge or spin ordering [14], which is also the case for Y123 [22].

3. Planar oxygen inequivalency

However, close examination of the planar oxygen spectra reveals substructure, non-existent at the apical site. In figure 3 there is an unambiguous splitting of the highest frequency satellite in our UD87 sample at temperatures above 100 K, in contrast to the corresponding lowest frequency satellite which has a much narrower linewidth. The spectrum at $T = 180$ K can be separated into two gaussian shaped peaks of equal weights (α and β). Consistent behavior was observed in UD79. Above 100 K we found that the full-width-at-half-maxima (FWHM) of the upper satellites were greater than for the lower satellites, figure 4, with a concomitant asymmetry in the satellite intensities figures 3 and 5. We take this as evidence for such a splitting even though it is unresolved. The asymmetry in the linewidths, i.e. comparison of high and low frequency satellites, can be accounted for by simultaneous spin and charge spatial modulations. Electronic order in only one of spin or charge channels is insufficient. Similar observations were reported by Wu *et al* [1, 4] from both ^{63}Cu and ^{17}O NMR for chain ordered Y123, and were interpreted as evidence for charge ordering, magnetic field induced ordering in that case. The maximum ^{17}O spectral splitting we have found in Hg1201 is ~60 kHz, similar to that reported for Y123 [4] where $\nu_Q \sim 0.9$ MHz.

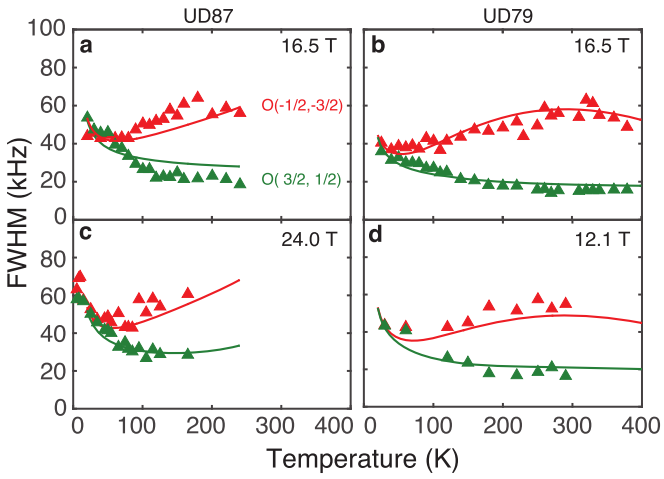

Figure 4. (a), (b) Anomalous asymmetry in the O(1) $(-1/2, -3/2)$ and O(1) $(3/2, 1/2)$ satellites as a function of temperature expressed by the full-width-at-half-maximum linewidth (FWHM) at various fields from 12.1 to 24 T. The solid lines are calculated from the parameters obtained from a global fit to the full set of spectral peaks using the model of two inequivalent planar oxygen sites (see text).

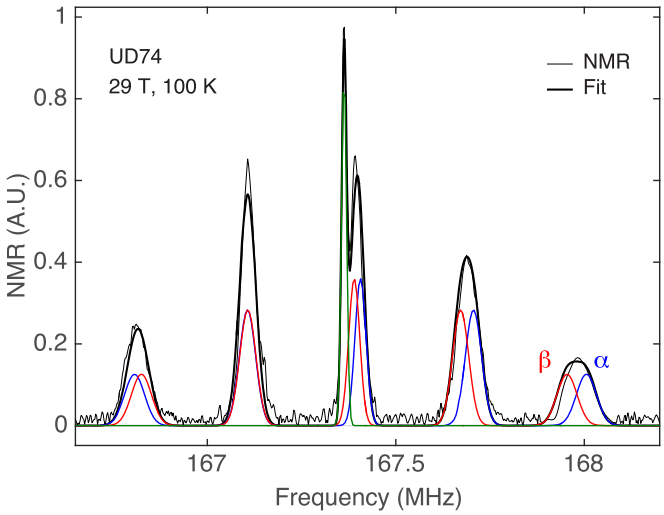

Figure 5. Two-site model fitting for UD74 spectra at 29 T and 100 K and $H_0||c$. The observed linewidth asymmetry is generated by a slight mismatch in magnetic and quadrupolar parameters between the two sites. The asymmetry is easily identified from the variation in the maximum intensity of the quadrupolar peaks. A sharp peak in the central site (green) is from the apical oxygen whose quadrupolar satellites occur with a larger ν_Q than can be displayed here.

Asymmetric distributions of quadrupolar satellite lineshapes can only arise under rather restrictive circumstances apart from possible electronic ordering. For example, misalignment of crystals relative to the magnetic field, or the existence of bi-crystal domains can result in an NMR spectral splitting. We investigated these possibilities, as discussed in section 6, using different models for analysis, and find that they do not account for our spectra.

4. Two-site model

It is most likely that the inequivalency of oxygen sites that we observe has a local origin associated with coexisting charge and spin density waves. The fact that the NMR satellites are asymmetrically affected requires that these modulations coexist, that they are coherent, and finally that they are locked in phase, as demonstrated by simulations presented later in section 5. Independent, or out of phase, superpositions of spin and charge order

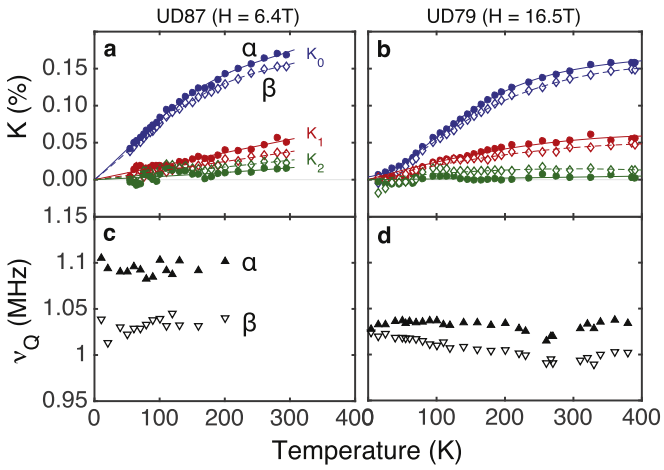

Figure 6. (a), (b) Temperature dependence of Knight shifts of the two inequivalent sites. The lines are guides to the eye. Error bars are smaller than the separation between α and β data at most temperatures. (c), (d) The separation of the satellites, ν_Q, is plotted as a function of temperature.

averaged over the sample destroy the asymmetry and broaden the NMR spectrum. Being intimately linked they must have the same origin. For simplicity we have analyzed our spectra in the context of a simple model of two inequivalent oxygen sites α and β in the CuO_2 plane having equal weight. Even if a spin or charge periodic order is incommensurate with the lattice it will be manifest in a prominent two-peak spectrum. In the following we describe our results using our model to determine the quadrupole frequency and Knight shift splittings which are a measure of the charge and spin density wave amplitudes respectively.

In order to explain the asymmetric linewidth distribution between the quadrupolar satellites, we used a two-site model assuming two, almost equivalent oxygen sites each characterized by a unique set of magnetic and quadrupolar parameters: $\nu_{Q,\alpha}$, $\nu_{Q,\beta}$, $K_{0,\alpha}$, $K_{1,\alpha}$, $K_{2,\alpha}$, $K_{0,\beta}$, $K_{1,\beta}$, $K_{2,\beta}$, σ_m, σ_q. The two sites are indicated by subscripts α and β. The principal axes for the two sites can be taken to be identical since we have investigated the possibility that this is not the case in section 6 called the bi-crystal model, and found that it does not account for our spectra.

$$A(f) = \sum_{m,i} A_{(m,m-1)} \exp\left(-\frac{(f - (f_{\mathrm{mag},i}(\theta, \phi) + f_{\mathrm{quad},i}(m, \theta, \phi)))^2}{2(\sigma_m^2 + (|m - 1/2|\sigma_q)^2)} \right). \quad (5)$$

Equation (5) represents NMR spectra for $I = \frac{5}{2}$ consistent with the quadrupolar Hamiltonian to first order for two inequivalent sites $i = \alpha, \beta$. The NMR amplitudes for symmetric pairs of upper and lower quadrupolar satellites are set to be equal, i.e., $A_{(-3/2,-1/2)} = A_{(1/2,3/2)}$ and $A_{(-5/2,-3/2)} = A_{(3/2,5/2)}$. The centroid of a quadrupolar pattern and the quadrupolar separations are given by, $f_{\mathrm{mag},i}$ and $f_{\mathrm{quad},i}$, with additional subscript designation for site distinction since each site generates its own full quadrupolar pattern. The magnetic and quadrupolar contributions to the total linewidth are represented as σ_m and σ_q, respectively, where each spectral peak is a gaussian with width σ taken as the sum in quadrature of the two contributions and where we note that the quadrupolar term is linearly incremented as the transition order increases, providing an unambiguous distinction between these two contributions. To calculate the FWHM linewidth we use 2.36 σ.

The uncertainties in determining frequency splittings from unresolved overlapping peaks is reduced by imposing mathematical constraints on the ten-gaussian fitting. We assumed that α and β peaks are gaussians of equal weight and width and that the magnetic and quadrupolar contributions are added in quadrature. We observed that the average Knight shift position of α and β peaks was magnetic field independent at two fields, $H_0 = 16.5$ and 30 T. Consequently, we constrained each Knight shift component to be magnetic field independent. An alternate model simulating the effect of sinusoidal spin and charge density waves will be discussed later in section 5. Analysis of all spectra was performed by fitting as required by equations (1)–(3). The NMR fit parameters are: $\nu_{Q,\alpha}$, $\nu_{Q,\beta}$, $K_{0,\alpha}$, $K_{1,\alpha}$, $K_{2,\alpha}$, $K_{0,\beta}$, $K_{1,\beta}$, $K_{2,\beta}$, σ_m, σ_q where the last two are magnetic and quadrupolar linewidths.

The results for several cases are shown in figure 6 with the linewidth components, σ_q and σ_m given separately in appendix B. We found that the Knight shifts were only weakly doping dependent, that σ_q was temperature independent and independent of field from 6.4 to 30 T, and that σ_m/H_0 followed a Curie-Weiss law. Using the fitting parameters, we were able to accurately simulate the spectra in figure 2. With these parameters, we calculated the FWHM linewidth of each composite peak shown as solid curves in figure 4. The consistency with

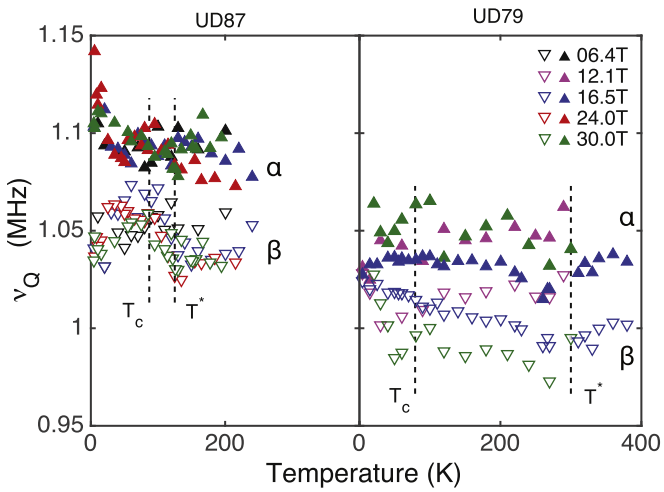

Figure 7. Temperature and field dependence of ν_Q is consistent with the existence of charge order manifest in the difference between α and β sites. There is no evidence for a field or temperature induced onset. Statistical errors in the plot are about ~13 kHz except the $H = 16.5$ T data for UD79 for which it is ~3 kHz where longer measurement times were possible. For a third sample, UD74, we only have data at 100 K but it is consistent with the above with $\Delta\nu_Q = 40$ kHz at both 21 and 24 T. The transition temperatures and pseudogap temperatures are shown by dashed vertical lines, $T^* = 125$ K for UD79, and 300 K for UD87, determined from our ^{63}Cu NMR T_1 relaxation measurements [20].

the raw data confirms the appropriateness for our model for two inequivalent oxygen sites. In addition, the partial splitting at the highest frequency satellite by ~60 kHz at $H_0 = 30$ T, shown in figure 3(c), agrees quantitatively with the calculated spectra based on the fitted parameters given by the solid black curve. It is important to note that the difference in the Knight shifts between alpha and beta sites decreases with decreasing temperature, mimicking the overall temperature dependence of the Knight shift, a well established manifestation of the effect of the pseudogap on the spin susceptibility for underdoped cuprates. Consequently the modulation of the Knight shift, coherent with the charge distribution modulation, can be directly attributed to the electronic spin susceptibility.

The quadrupolar frequency of each site is shown in figure 7 for all our data. A uniform field-independent difference $\Delta\nu_Q \equiv \nu_{Q,\alpha} - \nu_{Q,\beta} \sim 40$ kHz for α and β sites above ~100 K, is evident. In this range our measurements in Hg1201 indicate static electronic order. The general trend of increasing ν_Q with decreasing temperature can be attributed to temperature dependence of the lattice parameters. This interpretation can be made with more confidence using the apical site, analysis presented in section 7.

5. Numerical simulation

The effect of incommensurate spin and charge density wave modulations in the CuO_2 plane can be studied from simulation of the NMR spectra. In this case we consider 1D spin and charge density waves with the following equations.

$$A_S(x) = A_{S,0}\sin(2\pi x/\lambda_S + \phi_S), \tag{6}$$

$$A_C(x) = A_{C,0}\sin(2\pi x/\lambda_C + \phi_C). \tag{7}$$

The amplitudes of spin and charge density waves (SDW and CDW) are denoted by $A_{S,0}$ and $A_{C,0}$ where x is the distance in real space. For a coherent density wave modulation, $\lambda_S = \lambda_C = \lambda$. Incommensurability further requires λ to be an irrational multiple of the lattice constant. The phase of each wave is denoted by ϕ_S and ϕ_C giving a relative phase of $\phi = \phi_S - \phi_C$.

Density wave modulations induce a doublet splitting for all NMR peaks, corresponding to the α and β sites in the two-site model. Our numerical simulation of the effects of the spin and charge density waves in real space was sufficiently large that all the nuclei in a simulation cell provide ample sampling of the full spatial variation of the density waves. In the case of incommensurate modulations we define the probability density for frequency shifts that a nucleus experiences as follows:

$$P_S(H) = \int \delta(H - A_S(x))\,\mathrm{d}x, \tag{8}$$

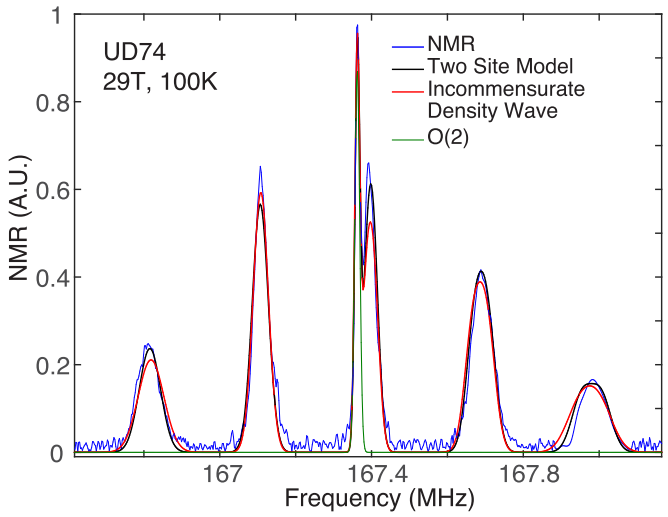

Figure 8. Comparison of the two-site model (black) introduced in section 4 and the incommensurate density wave simulation (red). Both can be fit to the experimental spectra with similar precision and the asymmetric lineshape distribution among the satellites is accurately represented.

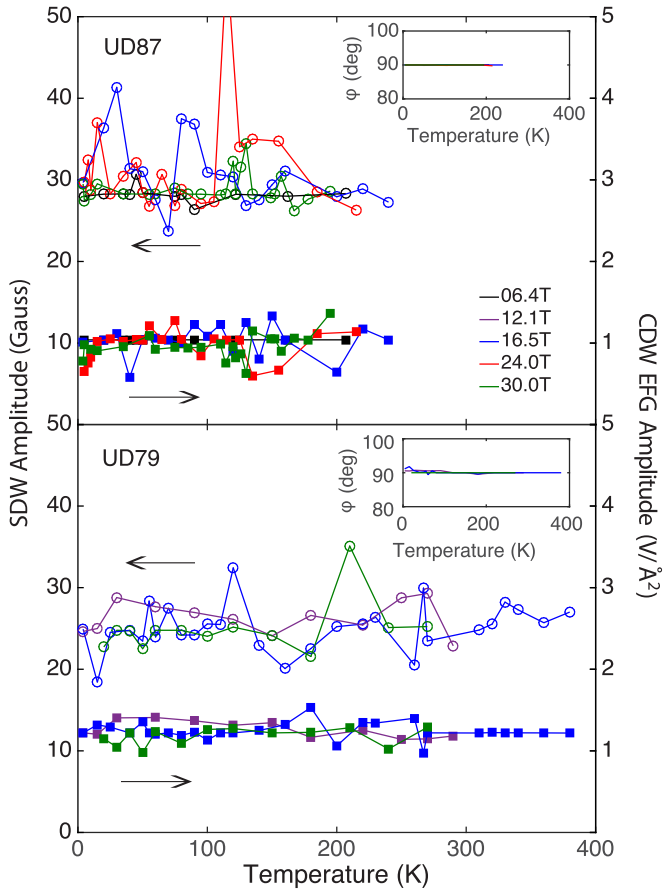

Figure 9. Amplitude of the SDW, $A_{S,0}$, and amplitude of the EFG, $2\pi A_{C,0}/\lambda$, determined from fitting all of the experimental spectra using the coherent incommensurate density wave model. This analysis show that both modulations are magnetic field and temperature independent with a well defined phase difference, ϕ, which is vanishingly small, indicating that CDW and SDW have a $\pi/2$ phase difference. The specific value of phase mismatch shown in the insets is robust showing little to no change throughout the range of field and temperature investigated.

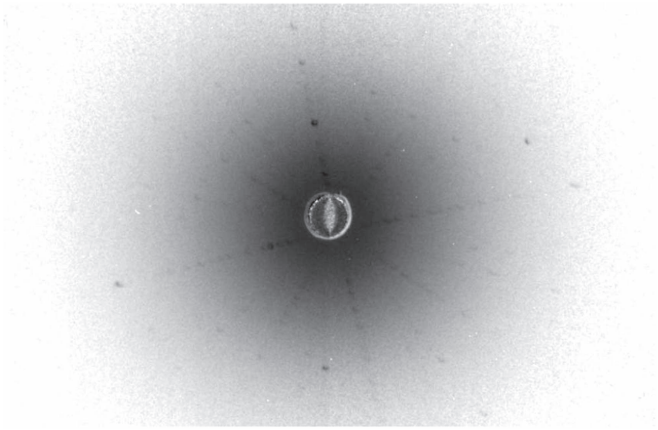

Figure 10. Laue image of the UD87 sample normal to the *c*-axis shows a single crystal domain consistent with the crystal structure of Hg1201. We have found no evidence of multiple crystal domains in the cation framework in any of our samples. Note however, that the x-ray Laue method is not sensitive to oxygen.

$$P_C(\nu_Q) = \int \delta\left(\nu_Q - \kappa \frac{\partial}{\partial x} A_C(x)\right) \mathrm{d}x. \tag{9}$$

where the crystal EFG scales linearly with ν_Q in the following equation,

$$\kappa = \frac{\mathrm{EFG}}{\nu_Q} = \frac{2I\,(2I-1)\,h}{3eQ}. \tag{10}$$

We have fit all our spectra for each sample using the model embodied in equations (1), (6)–(9) where the variables are, K_0, K_1, K_2, ν_Q, σ_S, σ_C, $A_{S,0}$, $A_{C,0}$, and ϕ, and the parameter, λ, is incommensurate with the lattice. An example of the calculated spectra resulting from this fit for UD74 is shown in figure 8 compared to the fit to the same data using the two-site model with very similar results.

This gives new insight. The relative phase angle, ϕ, and the magnitudes of SDW and CDW, $A_{S,0}$ and $A_{C,0}$, can be determined and are temperature independent. Interestingly, simulations such as this have not been discussed previously. According to our analysis, the relative phase $\pi/2$, is very robustly defined; see insets to figure 9. This phase mismatch between electronic density and spin density modulations has been predicted and observed in rather different circumstances, where it naturally occurs for Friedel type oscillations [25–27]. A relative phase of π has been found in topologically induced commensurate spin and charge modulations [28]. The magnitude of the EFG oscillation was found to be about 1 V Å^{-1}, less than 1% of the static EFG at the planar oxygen site in Hg1201. The magnitude of the SDW oscillation is ~27 Gauss, about an order of magnitude less than the incommensurate SDW observed in iron-pnictide superconductors [29], and might be related to the magnetism detected by polarized neutron scattering in the same material [30]. Note that the two-site model has an additional constraint imposed on the Knight shift such that it be magnetic field independent, an assumption based on direct measurement of the Knight shift at two magnetic fields.

The accuracies of our fitting analysis to the experimental spectra for the two-site model and the numerical simulation have similar statistics, i.e., χ^2, as shown in figure 8. Unfortunately, we cannot discriminate between them based solely on the fitting statistics.

6. Other scenarios: Bi-crystal model

The most straightforward causes of spectral splitting are (1) a simple misalignment of the magnetic field orientation, (2) the presence of different structural phases such as static octahedral buckling modes in cuprates [31], or (3) multiple crystal domains. We can eliminate the first case using a goniometer to map a rotation pattern and align the crystal *in situ* with high precision. If the sample consists of a bi-crystal, i.e. or two or more crystal domains, this could also produce a splitting of the spectra. However, the Laue diffraction images of our single crystals exclude existence of multiple crystal domains, figure 10.

Other mechanisms include existence of buckling of the CuO_2 plaquette. There have been reports of static buckling modes of the octahedra [32–39]. We have explored this possibility by attempting to fit the spectra with a ten-gaussian expression similar to the one in our two-site model. Instead of allowing two distinct sets of magnetic and quadrupolar parameters, we constrained the fitting to a single set of parameters for both sites while

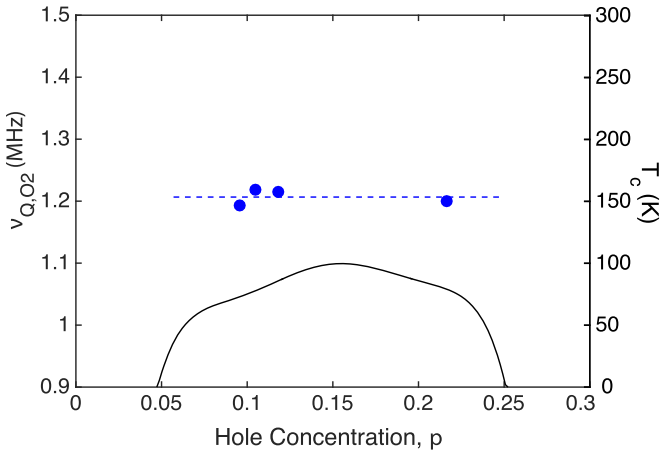

Figure 11. The quadrupolar frequency of apical oxygen in Hg1201 as a function of doping (blue, left). The right vertical axis corresponds to T_c in the superconducting dome [19].

allowing for a distinction between O(1a) and O(1b) to be manifest through different relative orientations of the principal axes for each crystal domain. The key difference between the two-site model and the bi-crystal model discussed in this section is that in the latter there are two distinct sets of principal axes whose relative orientations with respect to the magnetic field direction are expressed in terms of the spherical coordinates, $(\theta_i,\ \phi_i)$ as fit parameters which are different for $i = 1, 2$ where the index i specifies one of the two principal axis domains.

We found that this bi-crystal model does not fit our experimental spectra. In general, the compound spectra of a nearly degenerate pair of sites with the same principal axes (two-site model) has a larger linewidth for upper quadrupolar satellites only if the site with a larger magnetic shift also exhibits a larger quadrupolar shift so that both shift components constructively contribute to the total linewidth of the upper quadrupolar satellites. This is in contrast to the lower frequency satellites in which they compensate for one another resulting in a narrower linewidth. The bi-crystal model mostly predicts that a site with a larger magnetic shift has a smaller quadrupolar shift. This results in larger linewidth for lower quadrupolar satellites. An NMR spectral feature of this kind was observed experimentally in a low temperature orthorhombic phase of $La_{1.67}Eu_{0.2}Sr_{0.13}CuO_4$ [31]. However, this is inconsistent with our experiments. Additionally, a DFT simulation for Hg1201 excludes the existence of octahedra buckling modes which could otherwise generate a relevant scenario appropriate for the bi-crystal model [40].

Yet another possibility is the effect of interstitial dopant oxygens residing in the HgO plane. We have performed ^{199}Hg NMR, a nucleus that has been previously shown to be directly affected by the presence of the nearest neighbor dopant oxygen [16]. We have found that in all our Hg1201 single crystals the dopant oxygens are randomly distributed in the HgO plane with no bimodal effect that can result in a double peak splitting that is observed in the planar ^{17}O spectra of Hg1201 [20, 41]. Moreover, the quadrupolar frequency of the apical site is shown to be immune from doping variations over a wide range as shown in figure 11, indicating that the EFG in the CuO_2 plane is unlikely to be affected since it is much further away from the HgO plane than the apical oxygen.

The work by Haase, *et al* reports a similar quadrupolar asymmetry in ^{17}O NMR spectra obtained from aligned-powder samples of LSCO. They suggested that such a spectral feature may have been due to coherent spin and charge ordering [24, 42]. The limitations of their result, however, are inherently poor linewidth coming from aligned-powder samples and a more limited range of magnetic field of the data. In both LSCO and Hg1201 cases, this order does not seem to be influenced by either magnetic field or temperature. However, we exclude structural origins for the splitting in Hg1201 based on exceptionally narrow linewidth owing to the high quality single crystal samples and precision orientation alignment with a goniometer, which is not possible for an aligned powder.

7. Apical oxygen

Extending our earlier work [14] we have also studied ν_Q of the apical oxygen at $H = 30.0$ T (figure 12). The quadrupolar frequency is extracted from the quadrupolar separation of $\left(\pm\frac{3}{2},\ \pm\frac{5}{2}\right)$ satellite peaks. The average linewidth of each peak in the spectrum is ~10 kHz. The crystal EFG at the apical site scales linearly with ν_Q as

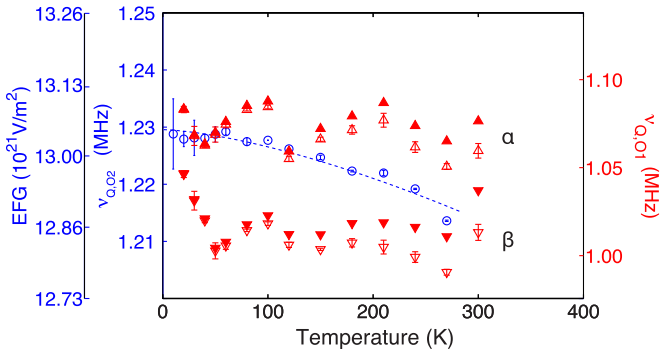

Figure 12. The phenomenological temperature dependence of lattice parameters for simple metals is shown by a dashed line. The origin of the decrease in ν_Q with increasing temperature at the apical site is therefore due to the temperature dependence of lattice parameters. The planar ν_Q for α and β sites in the two-site model for UD79 from figure 7 are shown after subtraction of this background temperature dependence. Solid (open) markers are after (before) the subtraction. Error bars are statistical.

shown in the following equation,

$$\mathrm{EFG} = \frac{\nu_Q 2I(2I-1)h}{3eQ}, \tag{11}$$

where Q is a nuclear quadrupolar moment. Our calculation of the crystal EFG at the apical site obtained from this analysis is consistent with first principle calculations for Hg1201 [43].

For non-cubic simple metals, the thermal response of the lattice parameters follows a phenomenological temperature dependence [44–46] which accounts for a contribution from the lattice vibrations due to phonon modes.

$$\nu_Q = \nu_{Q0}(1 - bT^{3/2}). \tag{12}$$

For the apical oxygen, we have observed a continuously decreasing EFG at the apical site with increasing temperature, figure 12, whose temperature dependence can be accounted for by this model with $\nu_{Q0} = 1.230$ (1) MHz and $b = 2.5(4) \times 10^{-6}\ \mathrm{K}^{2/3}$ in our UD79 sample. The thermal expansion of lattice parameters measured by neutron diffraction have a similar functional dependence [47].

The background dependence was subtracted from the planar data leaving only on-site lattice contributions to the EFG. The onset of an upturn of $\nu_{Q,\alpha}$ and $\nu_{Q,\beta}$ at a low temperature around 40 K corresponds to the vortex freezing temperature of this sample (UD79) which was separately determined from our NMR T_2 investigation of ^{63}Cu and ^{17}O [20]; however, the origin of this effect is unknown.

8. Conclusion

The magnetic and quadrupolar frequency shifts of ^{17}O NMR in cuprates can be associated with an intrinsic electronic instability with coherent charge and spin order in the CuO_2 plane. However, there is no evidence for a field or temperature induced onset, nor is there any correlation with vortex freezing (figure 1) or with the pseudogap. The change in ν_Q in UD87 below T_c at the β site might be a consequence of suppression of the CDW indicated by x-ray measurements [2, 3, 9]; however, this effect is not evident in sample UD79. It was suggested [4] that electronic ordering in Y123 fluctuates and that it is observed by NMR only when pinned, leading to an onset induced by a combination of sufficiently high magnetic field and sufficiently low temperature possibly associated with vortex freezing. This explanation does not account for magnetic field induced charge order observed in x-ray diffraction [5], nor does it correspond to our data for Hg1201. Identification of an onset of charge order, with no complementary spin order in Hg1201 was reported from resonant x-ray scattering [7] at the copper L_3-edge. This comparison provides a complementary view of charge ordering at different positions in the same material probed on different time scales. From x-ray diffraction in Hg1201 at optimal doping [8], evidence was found that oxygen interstitials induce formation of charge puddles in the CuO_2 plane, observations possibly related to the oxygen site inequivalency we report here.

Table A1. Knight shift and quadrupolar frequencies for the planar oxygen in underdoped Hg1201 single crystals at $H = 16.5$ T and $T = 80$ K (UD79) and $T = 100$ K (UD87). These results are associated with the average peak positions of α and β sites. Results for the underdoped $T_c = 74$ K (UD74K) crystal have been reported previously [14], including parameters for the apical oxygen (green solid curves in figure 2).

Sample	UD74K	UD79	UD87
K_0 (%)	0.056	0.055	0.078
K_1 (%)	0.018	0.0214	0.015
K_2 (%)	−0.01	0.0045	0.006
ν_Q (MHz)	1.05	1.0174	1.05
η	0.386	0.3738	0.385

Acknowledgments

We acknowledge contributions from Andrew Mounce, discussions with Marc-Henri Julien, and Vesna Mitrovic, and we thank Martin Greven for supplying the unprocessed Hg1201 crystals. Research was supported by the US Department of Energy, Office of Basic Energy Sciences, Division of Materials Sciences and Engineering under Awards DE-FG02-05ER46248 (Northwestern University). MKC is supported by funds from the US Department of Energy BES Grant No. LANLF100. A portion of this work was performed at the National High Magnetic Field Laboratory, which is supported by National Science Foundation Cooperative Agreement No. DMR-1157490 and the State of Florida.

Appendix A. Quadrupolar interactions

In the high field limit the quadrupolar interaction can be expanded for each eigenstate of the Hamiltonian using perturbation theory. The first order quadrupolar interaction for transition $(m, m-1)$ is given in equation (3). The second order interaction is described by the following equation.

$$\begin{aligned} f^{(2)}_{\text{quad}} = \frac{\nu_Q^2}{H_0\gamma}(1-\cos^2\theta)\times\Bigg[&\{102m(m-1)-18I(I+1)+39\} \\ &\times\cos^2\theta\left(1+\frac{2}{3}\eta\cos 2\phi\right)-\{6m(m-1)-2I(I+1)+3\}\left(1-\frac{2}{3}\eta\cos 2\phi\right)\Bigg] \\ &+\frac{\eta^2}{72}\frac{\nu_Q^2}{H_0\gamma}[24m(m-1)-4I(I+1)+9-\{30m(m-1)-2I(I+1)+12\}\cos^2\theta \\ &-\left\{\frac{51}{2}m(m-1)-\frac{9}{4}I(I+1)+\frac{39}{4}\right\}\cos^2 2\phi(\cos^2\theta-1)^2\Bigg]. \end{aligned} \tag{A1}$$

The magnitude of the second order term varies with the transition orders but it is generally less than ~1 kHz for the sample orientation, $H_0 \| c$. Our analysis in the main text, as well as our calculation of the linewidths shown in figure 4, include this second order interaction term. The angular dependence of all NMR peak frequencies is consistent with the known tetragonal structure of Hg1201 as measured by x-ray diffraction [48], and the crystal parameters extracted from this angular dependence are given in table A1.

Appendix B. Linewidth analysis of the inequivalent sites

There is a systematic behavior in the temperature dependence of linewidth components which emerges from the fitting analysis of experimental spectra. Figures B1–B3 show temperature and magnetic field dependence of the quadrupolar and magnetic linewidth contributions. The quadrupolar contribution was found to be temperature and magnetic field independent while the magnetic contribution increases with increasing field and decreasing temperature.

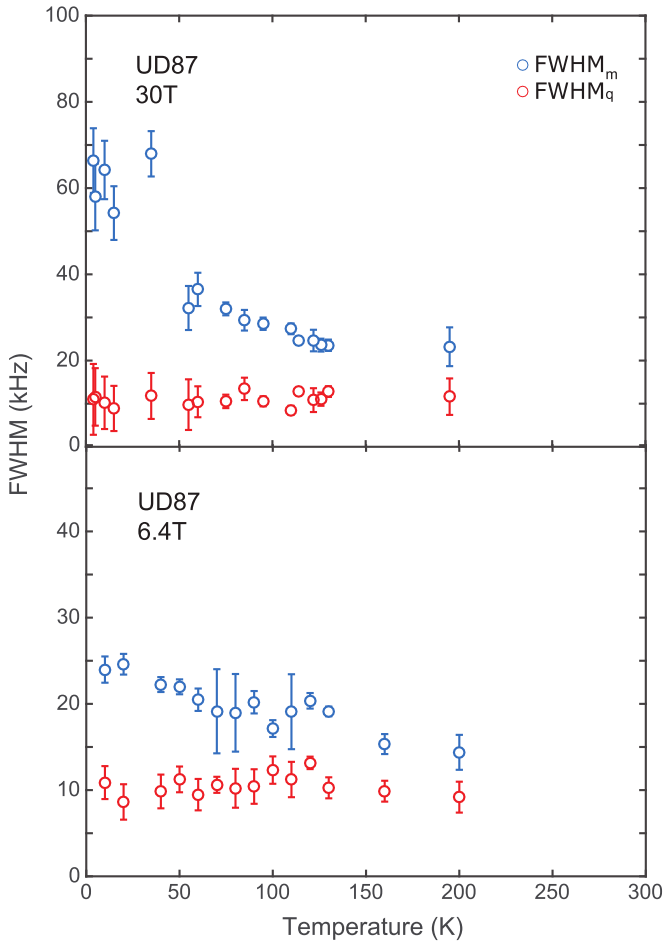

Figure B1. Magnetic and quadrupolar contributions to the total linewidth as a function of temperature obtained from the fitting. Error bars are statistical.

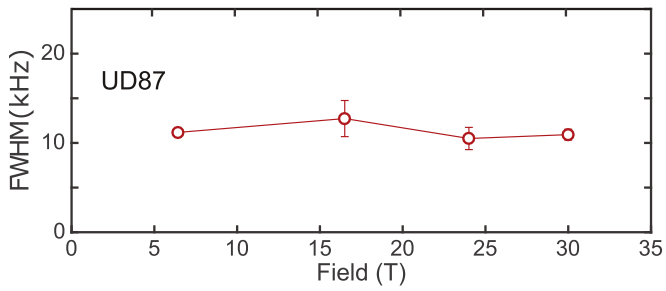

Figure B2. To get a linewidth that is representative of one field, we have averaged σ_q at all temperatures at that field. The error bars shown here are statistical.

The field and temperature dependence of σ_m for our two underdoped samples suggests Curie-Weiss behavior, shown in figures B1 and B3, where σ_m is divided by, γH, consistent with the equation,

$$\sigma_m(T, H) = \sigma_0 + \frac{CH}{T - \Theta}. \tag{B1}$$

The magnetic contributions for different fields coalesce into a common temperature dependence, that can be understood in terms of paramagnetic impurities as reported for Bi2212 [49] and Y123 [50].

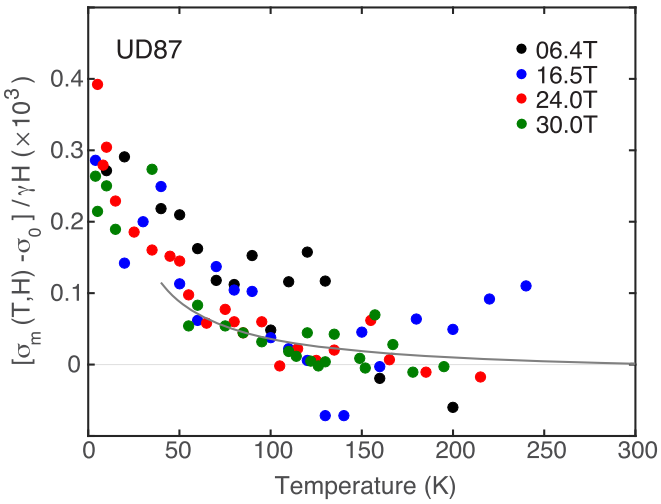

Figure B3. A single Curie-Weiss curve represents temperature and magnetic field dependence of the magnetic linewidth. In our underdoped samples the intrinsic linewidth is ~10 kHz, with the Curie-Weiss constant, $C = 30$ K T^{-1}, and the Curie-Weiss temperature, $\Theta \sim 0$ K. We have avoided fitting the magnetic contribution to the linewidth below the vortex freezing transition near $T = 40$ K.

References

[1] Wu T, Mayaffre H, Krämer S, Horvatić M, Berthier C, Hardy W N, Liang R, Bonn D A and Julien M-H 2011 *Nature* **477** 191
[2] Chang J *et al* 2012 *Nat. Phys.* **8** 871
[3] Ghiringhelli G *et al* 2012 *Science* **337** 821
[4] Wu T *et al* 2013 *Nat. Commun.* **4** 2113
[5] Gerber S *et al* 2015 *Science* **350** 949
[6] Keimer B, Kivelson S A, Norman M R, Uchida S and Zaanen J 2015 *Nature* **518** 179
[7] Tabis W *et al* 2014 *Nat. Commun.* **5** 5875
[8] Campi G *et al* 2015 *Nature* **525** 359
[9] Comin R and Damascelli A 2015 arXiv:1509.03313
[10] Taillefer L 2009 *J. Phys.* **21** 164212
[11] Doiron-Leyraud N *et al* 2013 *Phys. Rev.* X **3** 021019
[12] Doiron-Leyraud N, Proust C, LeBoeuf D, Levallois J, Bonnemaison J-B, Liang R, Bonn D, Hardy W and Taillefer L 2007 *Nature* **447** 565
[13] Barišić N *et al* 2013 *Nat. Phys.* **9** 761
[14] Mounce A M *et al* 2013 *Phys. Rev. Lett.* **111** 187003
[15] Li Y, Balédent V, Barišić N, Cho Y C, Sidis Y, Yu G, Zhao X, Bourges P and Greven M 2011 *Phys. Rev.* B **84** 224508
[16] Stern R, Heinmaa I, Pavlov D A and Bryntse I 2005 *New Challenges in Superconductivity* (Berlin: Springer) pp 69–72
[17] Mounce A M 2013 *PhD Thesis* Northwetsern University
[18] Lee J A 2016 *PhD Thesis* Northwetsern University
[19] Yamamoto A, Hu W and Tajima S 2000 *Phys. Rev.* B **63** 024504
[20] Lee J A, Xin Y, Stolt I, Halperin W P, Reyes A P, Kuhns P L and Chan M K 2017 *Phys. Rev.* B **95** 024512
[21] Carter G C, Bennett H and Kahan D J 1977 *Metallic Shifts in NMR* 1st edn (New York: Pergamon)
[22] Wu T, Mayaffre H, Krämer S, Horvatić M, Berthier C, Hardy W, Liang R, Bonn D and Julien M-H 2015 *Nat. Commun.* **6** 6438
[23] Kambe S, Yasuoka H, Hayashi A and Ueda Y 1993 *Phys. Rev.* B **47** 2825
[24] Haase J, Slichter C P, Stern R, Milling C T and Hinks D G 2000 *J. Supercond.* **13** 723
[25] Jena P, Singwi K S and Nieminen R M 1978 *Phys. Rev.* B **17** 301
[26] Manninen M, Jena P, Nieminen R M and Lee J K 1981 *Phys. Rev.* B **24** 7057
[27] Yu I and Halperin W P 1981 *J. Low Temp. Phys.* **45** 189
[28] Zachar O, Kivelson S and Emery V 1998 *Phys. Rev.* B **57** 1422
[29] Oh S, Mounce A M, Lee J A, Halperin W P, Zhang C L, Carr S, Dai P, Reyes A P and Kuhns P L 2013 *Phys. Rev.* B **88** 23
[30] Li Y, Balédent V, Barisić N, Cho Y, Fauqué B, Sidis Y, Yu G, Zhao X, Bourges P and Greven M 2008 *Nature* **455** 372
[31] Baek S and Hammel P C 2013 *Phys. Rev.* B **174505** 1
[32] Kirk M D, Nogami J, Baski A A, Mitzi D B, Kapitulnik A, Geballe T H and Quate C F 1988 *Science* **242** 1673
[33] Crawford M K, Farneth W E, McCarronn E M, Harlow R L and Moudden A H 1990 *Science* **250** 1390
[34] Pickett W E, Cohen R E and Krakauer H 1991 *Phys. Rev. Lett.* **67** 228
[35] Jepsen O, Andersen O K, Dasgupta I and Savrasov S 1998 *J. Phys. Chem. Solids* **59** 1718
[36] Chmaissem O, Jorgensen J D, Short S, Knizhnik A, Eckstein Y and Shaked H 1999 *Nature* **397** 45
[37] Dahm T 2000 *Phys. Rev.* B **61** 6381
[38] Bussmann-Holder A and Keller H 2005 *Eur. Phys. J.* B **44** 487
[39] Iwasawa H *et al* 2008 *Phys. Rev. Lett.* **101** 157005
[40] Gu K 2016 private communication
[41] Haase J, Rybicki D, Slichter C P, Greven M, Yu G, Li Y and Zhao X 2012 *Phys. Rev.* B **85** 104517
[42] Haase J, Slichter C P and Milling C T 2002 *J. Supercond.* **15** 339
[43] Correia J G, Araujo J P and Loureiro S M 2000 *Phys. Rev.* B **61** 11769

[44] Jena P 1976 *Phys. Rev. Lett.* **36** 418
[45] Christiansen J, Heubes P, Keitel R, Klinger W, Loeffler W, Sandner W and Witthuhn W 1976 *Z. Phys.* **24** 177
[46] Kaufmann E N and Vianden R J 1979 *Rev. Mod. Phys.* **51** 161
[47] Huang Q, Lynn J W, Xiong Q and Chu C W 1995 *Phys. Rev.* B **52** 462
[48] Zhao B X *et al* 2006 *Adv. Mater.* **18** 3243
[49] Chen B, Mukhopadhyay S, Halperin W P, Guptasarma P and Hinks D G 2008 *Phys. Rev.* B **77** 052508
[50] Bobroff J, Alloul H, Mendels P, Viallet V, Marucco J and Colson D 1997 *Phys. Rev. Lett.* **79** 3757